Wavelength Dependence of Atomic Excitation for Ar Subject to Intense Midinfrared Laser Pulses

Yang-Ni Liu(刘阳妮)[1,2], Song-Po Xu(许松坡)[2,4*], Mu-Feng Zhu(朱穆峰)[2,3], Zheng-Rong Xiao(肖峥嵘)[2,3], Shao-Gang Yu(余少刚)[2,4], Lin-Qiang Hua(华林强)[2,3], Xuan-Yang Lai(赖炫扬)[2,3,4], Wei Quan(全威)[2,3*], Wen-Xing Yang(杨文星)[1*], and Xiao-Jun Liu(柳晓军)[2,3*]

[1]*School of Physics and Optoelectronic Engineering, Yangtze University, Jingzhou 434022, China*
[2]*State Key Laboratory of Magnetic Resonance and Atomic and Molecular Physics, Wuhan Institute of Physics and Mathematics, Innovation Academy for Precision Measurement Science and Technology, Chinese Academy of Sciences, Wuhan 430071, China*
[3]*School of Physical Sciences, University of Chinese Academy of Sciences, Beijing 100049, China*
[4]*Wuhan Institute of Quantum Technology, Wuhan 430206, China*

(Received 17 July 2023; accepted manuscript online 31 August 2023)

We report experimental and theoretical investigations of wavelength dependence of Rydberg state excitation (RSE) process of Ar subject to intense laser fields. By simultaneously measuring ionization and RSE yields of Ar atoms subject to strong laser fields at a series of wavelengths, we obtain the wavelength scaling law of the ratio of Ar^* over Ar^+ with respect to the laser intensity, and this result can be well reproduced by a nonadiabatic model, but not by the classical-trajectory Monte Carlo model. Our results indicate that the nonadiabatic corrections of the photoelectron tunneling exit and tunneling probability play a significant role at shorter wavelengths. Analysis shows that the wavelength dependence phenomenon is due to the interplay of the nonadiabatic effect, wave-packet diffusion and Coulomb focusing effect of the liberated electron.

DOI: 10.1088/0256-307X/40/10/103201

Above-threshold ionization (ATI)[1–5] is a fundamental process of strong-field physics. As proposed by Keldysh,[6] ATI process can be well described in either the multiphoton or tunneling pictures. In addition to ionization, a substantial fraction of Rydberg atoms or molecules have been observed[7–17] and this phenomenon is usually dubbed as the Rydberg state excitation (RSE) process. The underlying mechanism of RSE can also be comprehended in pictures of multiphoton and tunneling. In the multiphoton scenario, Rydberg states are created via AC Stark-shifted multiphoton resonant excitation (MRE).[13–16] On the other hand, in the tunneling regime, it has been demonstrated that Rydberg states are formed through frustrated tunneling ionization (FTI).[7–12]

Compared to MRE, the mechanism of FTI attracts more attention. In the latter case, the tunneled electron does not gain sufficient energy in the laser field to escape the Coulomb potential of the parent ion and is eventually captured into a Rydberg state. It has been documented that the FTI mechanism is related to various physical phenomena, such as the acceleration of neutral particles,[8] the comprehension of some photoelectron spectral features (e.g., zero-energy structure),[18,19] and the near-threshold harmonics generation.[20,21]

Recently, on the other hand, observations beyond the FTI mechanism have also been documented. In 2017, Zimmermann *et al.*[13] investigated the intensity dependence of neutral atomic yield in the multiphoton regime at 400 nm and observed a sequence of steps, which can be attributed to closings of multi-photon ionization channels. In 2020, by measuring Ar^+ ions and Ar^* neutral atoms simultaneously, Xu *et al.*[15] observed a whole series of channel closings and firstly confirmed the predicted out-of-phase oscillation of excitation and ionization. In addition, Zhang *et al.*[14] provided a solid evidence of the MRE for the Rydberg fragments of molecules by an ultraviolet femtosecond laser pulse.

As stated above, the data measured at shorter wavelengths (e.g., 400 nm) show features closely related to MRE. With otherwise identical parameters, longer wavelength will lead to smaller Keldysh parameter[6] and the physical process can be better described in the tunneling picture. However, the atomic RSE process in the laser field with wavelength longer than 800 nm and even mid-infrared has not received enough attention. Since the Coulomb potential plays a non-negligible role in mid-infrared laser fields, exactly how and to which extent the Coulomb potential would affect the wavelength dependence of the RSE process is far from understood. Therefore, a systematic investigation of the wavelength dependence of RSE process is still in demand.

In this Letter, we present systematic experimental and theoretical investigations of the wavelength scaling of the atomic RSE process. Our observation relies on simultaneously measuring and comparing the intensity dependence of the yields of ions Ar^+ and excited neutral atoms Ar^*

*Corresponding authors. Email: spxu@apm.ac.cn; charlywing@wipm.ac.cn; wenxingyang2@126.com; xjliu@wipm.ac.cn
© 2023 Chinese Physical Society and IOP Publishing Ltd

at 800, 1300, 1500 and 1800 nm. The wavelength scaling law of the ratio of Ar^* over Ar^+ can be well reproduced by a nonadiabatic model, but not by the classical-trajectory Monte Carlo (CTMC) method. Our results indicate that the nonadiabatic corrections of the photoelectron tunneling exit and tunneling probability play a significant role at shorter wavelengths, while the nonadiabatic effect gradually becomes unimportant for longer wavelengths. Analysis shows that the wavelength dependence phenomenon is due to the interplay of the nonadiabatic effect, wave-packet diffusion and Coulomb focusing effect of the liberated electron.

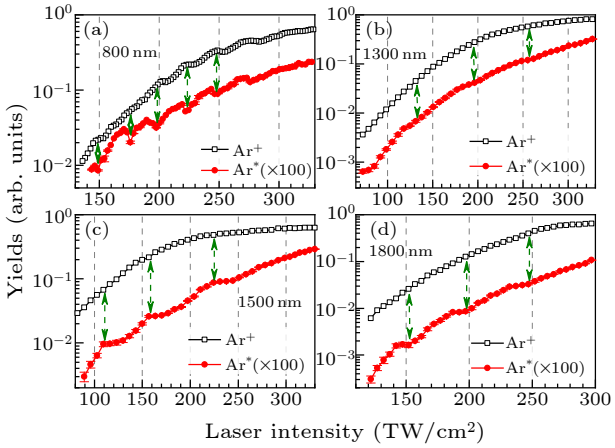

Fig. 1. The measured intensity dependence of Ar^+ (squares) and Ar^* (circles) yields at 800 nm (a), 1300 nm (b), 1500 nm (c) and 1800 nm (d). The intensities, at which steps happen, are indicated by green-dashed arrows.

In our experiments, wavelength-tunable midinfrared femtosecond laser pulses are generated by an optical parametric amplifier (TOPAS-C, Light Conversion, Inc.) pumped by a commercial Ti:sapphire laser system (Legend, Coherent, Inc.). The pulse length is $\sim$35 fs for signal pulse with the wavelengths of 800, 1300, and 1500 nm, and $\sim$55 fs for idler pulse of 1800 nm. The pulse energy from the optical parametric amplifier can be varied, before being focused into the vacuum chamber, by means of an achromatic half-wave plate followed by a polarizer. A collimated supersonic atomic beam of Ar crosses with the laser beam at the focal spot. The produced ion and neutral atom signals in the interaction point are registered by a home-made time-of-flight mass spectrometer.[22–25] At the interaction spot, pulsed and constant electric fields have been applied to a pair of electrodes (see Ref. [15] for more details). The laser intensity has been calibrated with the $10U_p$ (U_p is the ponderomotive energy of the laser field) cutoff of the above-threshold ionization spectra of Ar.[26]

In Fig. 1, the measured intensity dependence of the yields of Ar^+ ions and excited neutral Ar^* atoms with $n \leq 75$ at 800, 1300, and 1800 nm are presented. As is seen, the yields of Ar^+ ions and excited Ar^* atoms extend over several orders of magnitude as a function of the laser intensity. Moreover, the yields of Ar^+ ions and excited Ar^* atoms increase rapidly at lower intensity and smoothly at higher intensity and the yield of Ar^+ ions is about 2.5 orders of magnitude lager than the yield of Ar^* atoms. The yields of Ar^* exhibit prominent sequence of steps as a function of the laser intensity. According to Ref. [15], for 800 nm the steps can be attributed to channel closings, while at the longer wavelengths the interference of the contributions of different capture trajectories is responsible for the step structure observed.[11,12]

To describe the ultrafast dynamics more accurately, we perform numerical calculation with a nonadiabatic model, in which the nonadiabatic corrections of the tunneling exit and ionization rate have been employed.[27–32] In the calculation, we assume that the electron is released from a bound state to continuum through tunneling. Therefore, the following classical motion of the tunneled electron is described by the Newtonian equation

$$\frac{d^2\boldsymbol{r}}{dt^2} = -\boldsymbol{E}(t) - \nabla V(\boldsymbol{r}, t), \tag{1}$$

where $\boldsymbol{E}(t) = E_0 a(t)\cos(\omega t)\hat{z}$ is the linearly polarized laser electric field, with E_0 being the maximum of the laser field strength. The envelope function $a(t)$ contains two-cycle ramp-on exponentially, ten-cycle constant equal to 1 and two-cycle ramp-off exponentially to 0. Meanwhile, the Coulomb potential of Ar^+ is $V = -Z_{\text{eff}}/r$, with r denoting the distance between the tunneled electron and the parent ionic core and Z_{eff} being the effective nuclear charge.

The tunneled electron is assumed to have a zero initial longitudinal velocity and a nonzero initial transverse velocity with Gaussian distribution. Thus, the initial velocities of the electron are $v_{x0} = v_{\text{per}}\cos\theta$, $v_{y0} = v_{\text{per}}\sin\theta$ and $v_{z0} = 0$, where v_{per} is the transverse velocity, and θ is the angle between v_{per} and the x axis. The coordinate of the tunnel exit is (0, 0, z_0). The nonadiabatic correction factor z_0 is

$$z_0 = \frac{E(t_0)}{\omega^2}\left[1 - \sqrt{1+\gamma^2(t_0, v_{\text{per}})}\right]^{-1}, \tag{2}$$

where $\gamma(t_0, v_{\text{per}}) = \omega\sqrt{2I_p + v_{\text{per}}^2}/|E(t_0)|$ is the Keldysh parameter depending on the instantaneous tunneling time, and $E(t_0)$ is the initial instantaneous field.[29,30] The weight of each electron trajectory is given as

$$\Gamma(t_0, v_{\text{per}}) = \Gamma(t_0) \times \Omega(v_{\text{per}}),$$
$$\Omega(v_{\text{per}}) = \frac{v_{\text{per}}\sqrt{2I_p}}{|E(t_0)|}\exp\left[\frac{v_{\text{per}}^2\sqrt{2I_p}}{|E(t_0)|}\right].$$

The ionization rate $\Gamma(t_0)$ can be given by the Yudin–Ivanov formula[33]

$$\Gamma(t) = N(t)\exp\left[-\frac{E_0 a^2(t)}{\omega^3}\Phi(\gamma(t), \theta(t))\right], \tag{3}$$

where the nonadiabatic effect has been well considered, $\theta(t)$ is the phase of the laser electric field, and the function $\Phi(\gamma, \theta)$ is given by Eq. (12) in Ref. [33]. The preexponential factor is

$$N(t) = A_{n^*,l^*} B_{l,|m|}\left(\frac{3\kappa}{\gamma^3}\right)^{1/2} C I_p\left[\frac{2(2I_p)^{3/2}}{E(t)}\right]^{2n^*-|m|-1}. \tag{4}$$

Here, the coefficients A_{n^*,l^*} and $B_{l,|m|}$ come from the radial and angular parts of the wave function.[33] The factor

$C = (1+\gamma^2)^{|m|/2+3/4} A_m(\omega,\gamma)$ is the Perelomov–Popov–Terent'ev correction to the quasistatic limit $\gamma \ll 1$ of the Coulomb preexponential factor.[34]

With the classical Newtonian equations, the evolution of the tunneled or trapped electron is traced until $t_{\rm final}$, which denotes the time of laser pulse ends. An RSE event is identified when the energy of the tunneled electron is in the range between zero and ground state ionization potential at $t = t_{\rm final}$. In our calculations, 1×10^7 trajectories are launched with tunneling times randomly distributed inside the laser pulse for each wavelength.

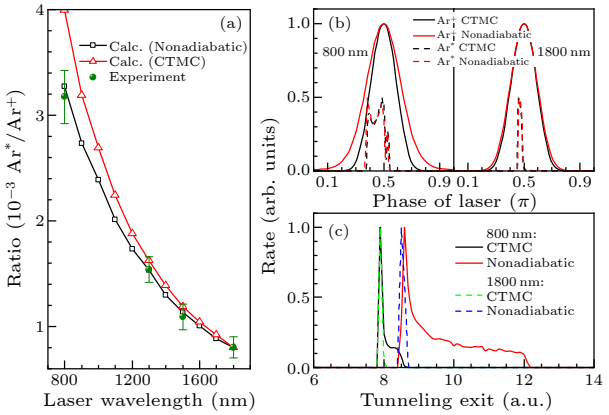

Fig. 2. (a) The measured intensity-averaged ratio of Ar^*/Ar^+ with respect of wavelength (olive circle), showing the calculated ratio of Ar^*/Ar^+ versus wavelength by the nonadiabatic model (black square) and the CTMC model (red triangle). (b) The ionization (solid) and excitation (dashed) rates versus the laser phase at the moment of tunnel ionization at 800 (left plot) and 1800 nm (right plot). (c) The excitation rates versus the tunnel exit with laser wavelengths of 800 (solid) and 1800 nm (dashed). The laser intensity is 200 TW/cm^2. See text for more details.

The measured intensity dependences of the ratio of Ar^*/Ar^+ at 800, 1300, 1500, and 1800 nm have been plotted in Fig. 2 of Ref. [12] and they exhibit pronounced oscillatory structure as a function of laser intensity. For different laser wavelengths, we employ different intensity ranges at a stable oscillation region to calculate the intensity-averaged ratios to study the wavelength dependence law rather than the ratio at a given intensity. The laser intensity ranges chosen are shown as the dashed rectangles in Fig. 2 of Ref. [12]. Here, the experimental wavelength dependence of intensity-averaged ratio Ar^*/Ar^+ as shown in Fig. 2(a). The calculated wavelength dependence of ratio Ar^*/Ar^+ based on the nonadiabatic model and the CTMC model are also presented in Fig. 2(a). We can see a good agreement between the measurements and the nonadiabatic model calculation. On the other hand, the ratio calculated by the CTMC model is significantly larger than the experimental result at 800 nm, and gradually converging with experimental results at 1800 nm. In addition, Fig. 2(b) shows the rate of ionization Ar^+ and excitation Ar^* as a function of the laser phase at the moment of tunnel ionization at 800 and 1800 nm with the forecast two models, respectively. At 800 nm, the ionization rate with the nonadiabatic model is notable larger than CTMC result, and the excitation rates with these two models are almost consistent. At 1800 nm, both of ionization and excitation rates are consistent for these two methods. Therefore, the nonadiabatic effect has a larger impact on short wavelengths, and plays a insignificant influence at 1800 nm. For example, the proportion of ionization rate with the nonadiabatic model becomes larger than the CTMC model, which can also explain why the ratio Ar^*/Ar^+ is smaller than the CTMC results at shorter wavelengths. As the laser wavelength increases, the range of ionization time increases, leading to a significant increase of the ionization rate, which also contributes to the wavelength-dependent results. Figure 2(c) shows the excitation rates as a function of the tunnel exit at 800 and 1800 nm with the nonadiabatic and CTMC methods, respectively. We can see that the nonadiabatic tunneling exit is further away from the core than semiclassical exit and the exit of 800 nm is larger than 1800 nm, which leads to a greater Coulomb potential effect for longer wavelength.

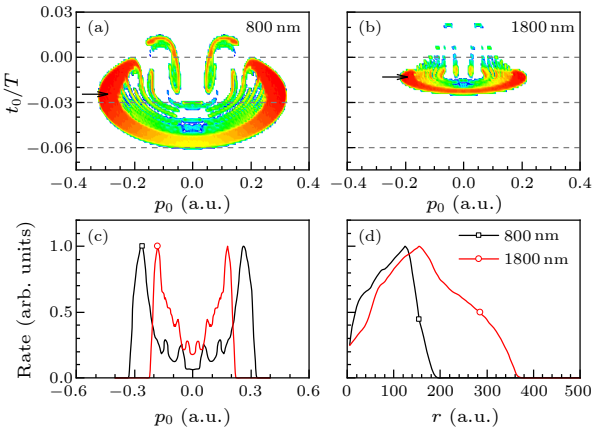

Fig. 3. [(a), (b)] The calculated Ar^* yield versus the tunneling ionization time t_0 and initial transverse momentum p_0 at 800 (a) and 1800 nm (b). (c) The excitation Ar^* yield with respect to the initial transverse momentum p_0. (d) The excitation Ar^* yield with respect to the distance between the photoelectron and the center of the Coulomb potential at $t = t_{\rm final}$. The laser intensity is 200 TW/cm^2. Here T is the laser optical period.

In order to reveal the physical insight behind the results presented in Fig. 2, we present the calculated Ar^* yield versus the tunneling ionization time t_0 and initial transverse momentum p_0 of the electrons captured into the Rydberg states in Figs. 3(a) and 3(b). In Fig. 3(a), the distribution exhibits a "crescent" shape[35,36] and the capture occurs for $|p_0| < 0.33$ a.u. and t_0 near the peak of laser field for 800 nm. As the laser wavelength increases, as shown in Fig. 3(b), the area of the distribution gradually becomes smaller and shifts towards the peak of laser field. The photoelectron initial transverse momentum distributions of RSE events have been shown in Fig. 3(c). As we can see, the initial transverse momentum distribution shows an obvious double-hump structure, and the interval between the two humps becomes smaller for longer wavelengths. This indicates that the Coulomb focusing effect decreases with increasing wavelength. Figure 3(d) shows

the Ar^* yield with respect to the distance between the photoelectron and core. As we can see, right after the end of the laser pulse, the recaptured photoelectrons are closer to the ionic core in the case of shorter wavelengths. Specifically, the maximum distances of the photoelectrons associated with the RSE from the core are 190 a.u. for 800 nm and 375 a.u. for 1800 nm, respectively. These results can be qualitatively understood by the stronger diffusion of the electron wave-packet for longer wavelengths.

The analysis can help us to comprehend the mechanism of RSE process better. The electron with energy of $E_{\rm final} < 0$, where $E_{\rm final} = \frac{p^2}{2} - \frac{Z_{\rm eff}}{r}$ is the electron energy at $t = t_{\rm final}$, can be recaptured in the Rydberg state. For longer wavelength, the electron quiver amplitude is larger, which leads to a further electron spatial distributions and weaker Coulomb potential. This illustrates the increase of the wave-packet diffusion effect with increasing wavelength. On the other hand, the transverse momentum of recaptured electron could be smaller due to the weaker Coulomb potential for longer wavelength. Obviously, the effects of wave-packet diffusion and Coulomb focusing are both important in the wavelength-dependence atomic excitation phenomenon.

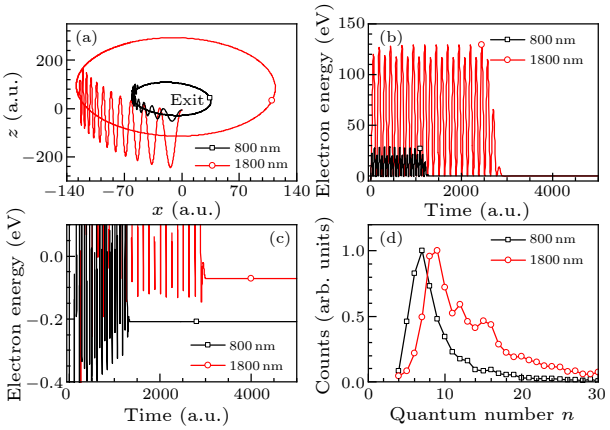

Fig. 4. (a) Typical trajectories calculated for the two wavelengths with otherwise identical conditions indicated by black arrows in Figs. 2(a) and 2(b). (b) The temporal evolution of electron energy of the two trajectories above. (c) The same data in (b) with the energy interval of $[-0.4, 0.1\,{\rm eV}]$. (d) The principle quantum number (n) distribution of the RSE population after laser pulse ends for 800 and 1800 nm. The laser intensity is $200\,{\rm TW/cm^2}$. In the calculation, the electron orbit is traced until $t = t_{\rm final} + 100T$.

To further explore the mechanism of atomic RSE in the mid-infrared laser fields, two typical trajectories with identical initial conditions [indicated by black arrows in Figs. 3(a) and 3(b)] except for wavelength have been pictured in Fig. 4(a). It is shown that, for wavelengths of 800 and 1800 nm, the tunneled electron oscillate along with the laser field until it ends and is then captured in an elliptical orbit. The orbital radius is larger for longer wavelength and larger radius usually corresponds to the Rydberg state with higher principle quantum number. In Fig. 4(b), the temporal evolution of electron energies of the two orbits have been presented and the region of energy less than 0 has been shown more clearly in Fig. 4(c). We can see that the energies of the both orbits are less than 0 when $t > t_{\rm final}$ and higher for the longer wavelength (e.g., $-0.21\,{\rm eV}$ for 800 nm, $-0.072\,{\rm eV}$ for 1800 nm). Generally, the principal quantum number n of the Rydberg states can be determined according to the energy of the electron after being captured (i.e., $n \sim \sqrt{I_{\rm p}/2|E_{\rm p}|}$, where $E_{\rm p}$ is the electron energy at $t_{\rm final}$).[36,37] In Fig. 4(d), we show the n distribution of excited Ar^* atoms for the two wavelengths. We can see that the distribution shifts to the higher n direction with rising wavelength. Indeed, the peak appears around $n = 7$ and $n = 9$ for 800 nm and 1800 nm, respectively.

In conclusion, we have performed a joint experimental and theoretical investigation on the wavelength dependence of the atomic RSE process. Our observation relies on simultaneously measuring and comparing the intensity dependence of the yields of ions Ar^+ and excited neutral atoms Ar^* at 800, 1300, 1500, and 1800 nm. The wavelength scaling law of the ratio of Ar^* over Ar^+ with respect to the laser intensity can be well reproduced by the nonadiabatic model, but not by the CTMC model. Our results indicate that the nonadiabatic corrections of the photoelectron tunneling exit and tunneling probability play a significant role at shorter wavelengths, while the nonadiabatic effect gradually becomes unimportant for longer wavelengths. Analysis shows that the wavelength dependence phenomenon is due to the interplay of the nonadiabatic effect, wave-packet diffusion and Coulomb focusing effect of the liberated electron. Our work sheds new light on establishing a comprehension for the atomic dynamics in strong laser fields.

Acknowledgement. Supported by the National Key Research and Development Program of China (Grant No. 2019YFA0307700), the National Natural Science Foundation of China (Grant Nos. 12004391, 12104465, 12274420, and U21A20435), China Postdoctoral Science Foundation (Grant Nos. 2019M662752, 2020T130682, and 2022M713219), CAS Project for Young Scientists in Basic Research (Grant No. YSBR-055), the Science and Technology Department of Hubei Province (Grant No. 2020CFA029), Knowledge Innovation Program of Wuhan-Shuguang Project (Grant No. 2022020801020140), and K. C. Wong Education Foundation.

References

[1] Agostini P, Fabre F, Mainfray G *et al.* 1979 *Phys. Rev. Lett.* **42** 1127
[2] de Boer M P and Muller H G 1992 *Phys. Rev. Lett.* **68** 2747
[3] DiMauro L F and Agostini P 1995 *Adv. At. Mol. Opt. Phys.* **35** 79
[4] Becker W, Grasbon F, Kopold R *et al.* 2002 *Adv. At. Mol. Opt. Phys.* **48** 35
[5] Agostini P and DiMauro L F 2008 *Contemp. Phys.* **49** 179
[6] Keldysh L V 1965 *Sov. Phys. Usp.* **8** 496
[7] Nubbemeyer T *et al.* 2008 *Phys. Rev. Lett.* **101** 233001
[8] Eichmann U, Nubbemeyer T, Rottke H *et al.* 2009 *Nature* **461** 1261
[9] Eichmann U, Saenz A, Eilzer S *et al.* 2013 *Phys. Rev. Lett.* **110** 203002

[10] Zimmermann H, Buller J, Eilzer S *et al.* 2015 *Phys. Rev. Lett.* **114** 123003
[11] Liu M Q, Xu S P, Hu S L *et al.* 2021 *Optica* **8** 765
[12] Xu S P, Liu M Q, Quan W *et al.* 2022 *Phys. Rev. A* **106** 063106
[13] Zimmermann H, Patchkovskii S, Ivanov M *et al.* 2017 *Phys. Rev. Lett.* **118** 013003
[14] Zhang W B *et al.* 2019 *Nat. Commun.* **10** 757
[15] Xu S P, Liu M Q, Hu S L *et al.* 2020 *Phys. Rev. A* **102** 043104
[16] Chetty D, Glover R D, deHarak B A *et al.* 2020 *Phys. Rev. A* **101** 053402
[17] Hu S L, Hao X L, Lv H *et al.* 2019 *Opt. Express* **27** 31629
[18] von Veltheim A, Manschwetus B, Quan W *et al.* 2013 *Phys. Rev. Lett.* **110** 023001
[19] Wolter B, Lemell C, Baudisch M *et al.* 2014 *Phys. Rev. A* **90** 063424
[20] Beaulieu S, Camp S, Descamps D *et al.* 2016 *Phys. Rev. Lett.* **117** 203001
[21] Yun H, Mun J H, Hwang S I *et al.* 2018 *Nat. Photon.* **12** 620
[22] Wiley W C and McLaren I H 1955 *Rev. Sci. Instrum.* **26** 1150
[23] Guilhaus M, Selby D, and Mlynski V 2000 *Mass Spectrom. Rev.* **19** 65
[24] Cheng J X, Ouyang X P, Zheng Y *et al.* 2008 *Chin. Phys. B* **17** 02881
[25] Zhang P, Feng Z P, Luo S Q *et al.* 2016 *Chin. Phys. B* **25** 033202
[26] Grasbon F, Paulus G G, Walther H *et al.* 2003 *Phys. Rev. Lett.* **91** 173003
[27] Song X H, Lin C, Sheng Z H *et al.* 2016 *Sci. Rep.* **6** 28392
[28] Yang W F, Zhang H T, Lin C *et al.* 2016 *Phys. Rev. A* **94** 043419
[29] Li M, Geng J W, Han M *et al.* 2016 *Phys. Rev. A* **93** 013402
[30] Li M, Liu M M, Geng J W *et al.* 2017 *Phys. Rev. A* **95** 053425
[31] Liu M M, Li M, Shao Y *et al.* 2017 *Phys. Rev. A* **96** 043410
[32] Luo S Q, Li M, Xie W H *et al.* 2019 *Phys. Rev. A* **99** 053422
[33] Yudin G L and Ivanov M Y 2001 *Phys. Rev. A* **64** 013409
[34] Perelomov A M, Popov V S, and Terent'ev M V 1966 *Sov. Phys. JETP* **23** 924
[35] Liu H *et al.* 2012 *Phys. Rev. Lett.* **109** 093001
[36] Shvetsov-Shilovski N I, Goreslavski S P, Popruzhenko S V *et al.* 2009 *Laser Phys.* **19** 1550
[37] Eilzer S and Eichmann U 2014 *J. Phys. B* **47** 204014